A novel face-centered cubic high-entropy alloy strengthened by

nanoscale precipitates

 $Ruirun\ Chen^{1,\,2^*},\ Gang\ Qin^1,\ Peter\ K.\ Liaw^3,\ Yanfei\ Gao^3,\ Huiting\ Zheng^1,\ Liang\ Wang^1,\ Yanqing\ Mang^2,\ Yanqing\ Mang^2,\ Manqing\ Mang^2,\ Manqing\ Manq^2,\ Manqing\ Manqing\$

Su¹, Hongsheng Ding¹, Jingjie Guo¹, Hengzhi Fu¹

1, National Key Laboratory for Precision Hot Processing of Metals, Harbin Institute of Technology, 150001, China

2, State Key Laboratory of Advanced Welding and Joining, Harbin Institute of Technology, 150001, China

3, Department of Materials Science and Engineering, The University of Tennessee, Knoxville, TN 37996, USA

*Corresponding author. Tel. /Fax: +86-451-86412394; Email address: ruirunchen@hit.edu.cn

Abstract

A new single phase face-centered cubic (FCC) Co₉Cr₇Cu₃₆Mn₂₅Ni₂₃ (at.%, similar hereinafter) high-entropy alloy (HEA) was prepared by melting. A mass of nano-precipitates with several nanometers was uniformly distributed in this alloy. The tensile yield strength, ultimate tensile strength, tensile elongation were tested as 401MPa, 700MPa and 36% respectively. EDS results show that the nano-precipitates are rich in Co and Cr elements. In addition, the crystal-forming behavior and the nanoscale precipitates forming mechanism were revealed.

Keywords: High-entropy alloys; Crystal growth; Microstructures; Mechanical properties

High-entropy alloys (HEAs) contain at least four principal elements and were first proposed by Yeh, J.W. and Cantor in 2004 [1, 2]. Today, it continues to attract extensive

research attention due to its excellent mechanical properties and simple face-centered cubic and body-centered cubic (FCC/BCC) solid solutions structure [3-15]. Several studies about mechanical properties [16], phase transformation [17], phase predictions [18-31], and phase stability [32-34] of HEA had been reported from 2015 to 2017.

In addition, Ma et al. investigated the effect of cooling rate on microstructure and mechanical properties of Al_xSi_{0.2}CrFeCoNiCu_{1-x} HEA, and they found that the high cooling rate restricts the growing space of grains by stimulating more potential nucleation sites for the primary phase [35]. The effect of atomic size on the type of major intermetallic phase was also studied by Tsai et al. in 2007, and they found that atomic size difference is a key factor in the selection of major intermetallic phase type [36]. Huo et al. investigated the strain-rate effect on the tensile behavior of CoCrFeNi HEAs, and they found that the tensile strength and ductility of the said HEA increased along with increasing strain rate and that the dominant deformation mechanism shifted from the dislocation motion at the lower strain rates to stacking faults at the higher strain rates [37]. Furthermore, Liu N et al. studied the rapid solidification behavior of CoCrCuFexNi HEAs and summarized the correlation between undercooling and microstructures [38]. Evidently, HEA has been a popular direction in materials filed. However, researches on phase-forming behavior in HEA are limited. In this paper, we introduce a novel Co₉Cr₇Cu₃₆Mn₂₅Ni₂₃ (at. %) HEA. The mechanical properties, phase composition, microstructure, and component distribution of the proposed HEA were characterized. An atom motion model was set up to describe the behavior of crystal-forming and nanometer precipitates-forming in the proposed HEA.

The alloy was obtained by melting pure metals (purity> 99.8 wt. %) by arc melting under high-purity argon state and was smelted seven times to ensure chemical homogeneity. X-ray diffraction (XRD) using CuKα radiation (MXP21VAHF) was utilized to identify the phase structures of HEAs. Scanning electron microscopy (SEM) and transmission electron microscopy (TEM) were used to characterize the microstructure morphology. Moreover, energy dispersive spectrometer (EDS) was used to inspect the element distribution. For microstructure observation, the samples were sequentially ground and polished and then underwent electropolishing in a mixture of 90% acetic acid and 10% perchloric acid at room temperature with an applied voltage of 27 V for 15 seconds. Flat specimens, with thickness of 1 mm and gauge length and width of 10 mm and 2 mm, respectively, underwent tensile testing at a strain rate of 0.6 mm/min at room temperature. The strain was accomplished using an extensometer.

Figure 1 shows the mechanical behavior and crystal structure of Co₉Cr₇Cu₃₆Mn₂₅Ni₂₃ HEA. It shows HEA. Figure 1 (a) presents the XRD patterns of Co₉Cr₇Cu₃₆Mn₂₅Ni₂₃ HEA. It shows that the Co₉Cr₇Cu₃₆Mn₂₅Ni₂₃ HEA has two crystal structure, FCC(225, Cu riched) and FCC (225, Co and Cr riched) crystal structure (Comprehensive analysis with the elements distribution maps). Figure 1 (b) shows the tensile engineering stress–strain curve, in which the tensile yield strength is 401 MPa, the ultimate strength is 700 MPa, and the elongation is 36%.

The tensile yield strength, ultimate tensile strength and elongation for the Co₉Cr₇Cu₃₆Mn₂₅Ni₂₃ HEA and other HEAs were presented in Figure 1 (c) and (d) [10,

^{12, 15, 46-53}]. Which shows that the tensile yield strength and elongation have a good combination, while hase no advantage in the ultimate tensile strength.

For a more intense investigation on the phase-forming behavior of the proposed HEA system. Microstructure attained by SEM and elements distribution maps of Co₉Cr₇Cu₃₆Mn₂₅Ni₂₃ HEA through EDS were shown in Figure. 2. The crystal grains appeared to be peritectic-structure with a core on the inside (see Figure. 2 (a)). The EDS maps (see Figure. 2 (b-f)) revealed that a large number of Co and Cr elements with higher melting point segregations existed in the primary phase area; however, the Cu element, which has a lower melting point, was scanty in this area. The Ni and Mn elements were lightly segregated in the primary phase and crystal areas, respectively. The abovementioned results demonstrate the relationship between melting point of alloy elements and phase-forming order. These cores were used as the primary phase; the atoms with lower melting point attached themselves to the primary phase based on the original arrangement mode, which prompted the grains to gradually increase in size and form a whole grain without changing the crystal structure.

To clearly observe the nanometer precipitates and identify their crystalline structure, the sample was observed through TEM. As shown in Figure. 4(a), a mass of nanometer precipitates were found in the $Co_9Cr_7Cu_{36}Mn_{25}Ni_{23}$ HEA. The nanometer precipitates, which were several nanometers in size, were diffusely distributed in the matrix. The electron diffraction spot illustrated in Fig. 4(b) shows that the proposed HEA has a single FCC (1 $\overline{2}$ $\overline{2}$) crystalline structure. Figures 4(c) and (d) show the bright-field TEM image with high magnification and the corresponding electron

nm in diameter and have a FCC (1 1 1) structure. Figures 4(e-j) show the HAADF image and the corresponding STEM-EDS elemental maps of Co, Cr, Cu, Mn, and Ni, which reveals that the nanometer precipitates were rich with Co and Cr elements but not with Cu. The nanometer precipitates were mainly generated as the solid solubility of the elements Co and Cr in the matrix were decreased when the temperature dropped and when a part of the atoms of these elements were separated from the supersaturated solid solution as well. As mentioned before, there has been difficulty in increasing the size of the grain due to the sluggish diffusion effect and the formation of nanometer precipitates. Furthermore, a mass of nanometer precipitate is pivotal in improving the strength of the proposed HEA, which demonstrated greater strength as compared to others FCC HEAs.

As shown in Figure. 4(a), an atom motion model was set up to describe the crystal-forming behavior in HEA. The atoms with higher melting point (Co, Cr, and Ni) preferentially precipitated as the primary phase when mixed with small amount of atoms with low melting points (Cu and Mn) as the temperature decreased: this observation can be verified through the elements distribution maps presented in Figure. 2. When the temperature was further reduced, the atoms with lower melting points separated out attached themselves to the primary phase, which prompted the grains to gradually increase in size and form a whole grain with peritectic-structure (as shown in Figure. 4(a)). After the liquid metal solidified and as the temperature dropped, the Co and Cr atoms were separated from the supersaturated solid solution.

Moreover, there has been difficulty in increasing the size of the precipitated phase due to sluggish diffusion effect and forming nanometer precipitates (as shown in Figure. 4(b)).

 ΔS_{mix} (entropy of mixing), ΔH_{mix} (enthalpy of mixing), T_m (The average melting point), Ω (the scald ratio of ΔS_{mix} to ΔH_{mix}), δ (atomic size difference), and VEC (valence electron concentration), these physical parameters are considered as the key factor for predicting the structural stability and phase formation in HEAs $^{[5,\,21-31,\,39-42]}$. Yang and Zhang proposed that when $\Omega \geq 1.1$ and $\delta \leq 6.6\%$, the stable solid-solution phase is formed in multi-component HEA systems $^{[5,\,21,\,23,\,42]}$. δ (atomic size difference) can be attained by equation $(1)^{[5,\,21,\,23,\,41,\,42]}$.

$$\delta = \sqrt{\sum_{n=1}^{n} c_i (1 - \frac{r_i}{\sum_{n=1}^{n} (c_i r_i)^2})^2}$$
 (1)

Where r_i is the atomic radius of the *i*th constituent element, c_i represents the atomic percentage of the *i*th component element, based on equation (1), the δ (atomic size difference) of $\text{Co}_9\text{Cr}_7\text{Cu}_{36}\text{Mn}_{25}\text{Ni}_{23}$ HEA is 3.1%.

 Ω is the scald ratio of ΔS_{mix} to ΔH_{mix} , it can be attained by equation (2) [5, 21, 23, 41, 42].

$$\Omega = \frac{T_m \Delta S_{mix}}{|\Delta H_{mix}|} \tag{2}$$

Where T_m is the average melting point, ΔS_{mix} is the entropy of mixing, ΔH_{mix} is the enthalpy of mixing.

 T_m can be calculated by equation (3) [5, 21, 23, 41, 42].

$$T_m = \sum_{n=1}^{n} (c_i(T_m)_i)$$
 (3)

Where n represents the number of component elements, $(T_m)_i$ is the melting point of the ith constituent element.

 ΔH_{mix} can be calculated by equation (4) [5, 21, 23, 41, 42].

$$\Delta H_{mix} = \sum_{n=1}^{n} \Omega_{ij} c_i c_{j_{i \neq j}}$$
 (4)

Where Ω_{ij} usually equals to $4 \Delta Hij^{mix}$, where ΔHij^{mix} is the enthalpy of mixing of the *i*th and *j*th component element, it can be attained in this paper [39].

 ΔS_{mix} can be calculated by equation (5) [5, 21, 23, 41, 42].

$$\Delta S_{mix} = -R \sum_{n=1}^{n} (c_i \ln c_i)$$
 (5)

Where R is the universal gas constant (8.314 kJ⁻¹ mol⁻¹), based on equations (2-5), the Ω (the scald ratio of ΔS_{mix} to ΔH_{mix}) of $Co_9Cr_7Cu_{36}Mn_{25}Ni_{23}$ HEA is 9286.6. According to the criterion of Yang and Zhang ^[23], the $Co_9Cr_7Cu_{36}Mn_{25}Ni_{23}$ HEA should be a stable solid-solution phase, which agree with the prediction.

Guo et al. reported that VEC is another important parameter for predicting phase structure of HEA $^{[24-26]}$. The criterion is that a sole solid-solution phase with an FCC structure is formed when VEC \geq 8, both the FCC and BCC structured solid-solution phases are denatured when $6.87 \leq \text{VEC} < 8$, a single BCC solid-solution phase is present when VEC $< 6.87^{[24-26]}$. Tsai et al. proposed that σ phase was formed when alloys having VEC values between 6.88 and 7.84 either in the as-cast state or during aging at suitable temperatures $^{[28,29]}$. In addition, our previous studies also exhibited that, element with a VEC lower than the average VEC of the matrix is added in HEA, it is helpful to improve the strength, while ductility could be improved by selecting another element with a VEC higher than the average VEC for the matrix $^{[43-45]}$.

VEC can be calculated by equation (6) [24-26, 28, 29, 43-49].

$$VEC = \sum_{n=1}^{n} c_i (VEC)_i \tag{6}$$

Where $(VEC)_i$ is the VEC of the *i*th component element. Based on equation (6), the VEC (valence electron concentration) of Co₉Cr₇Cu₃₆Mn₂₅Ni₂₃ HEA is 9.24.

According to the criterion of Guo et al. and Tsai et al. [24-26, 28, 29], the Co₉Cr₇Cu₃₆Mn₂₅Ni₂₃ HEA would form a stable single FCC solid-solution phase, the experimental result agrees with the prediction.

We are the first to investigate the Co₉Cr₇Cu₃₆Mn₂₅Ni₂₃ HEA. Our proposed HEA had the tensile yield strength and ultimate strength was 401 MPa and 700 MPa, respectively; the tensile elongation was 36%. A mass of super-nanoscale precipitates, which were several nanometers (3-8 nm) in size, abundant in Co and Cr, and scarce in Cu, were found in the novel HEA. Based on the EDS analysis result, in the crystal-forming behavior of HEA, the atoms with higher melting points preferentially precipitated as the primary phase whereas atoms with lower melting points were separated out and attached themselves to the primary phase as the temperature was reduced. This prompted the grains to gradually increase in size and form a whole grain. As the temperature dropped, a part of atoms of Co and Cr were separated from the supersaturated solid solution, which, on the other hand, encountered difficulty in increasing its size due to the sluggish diffusion effect and the forming nanometer precipitates.

Acknowledgement

The present work was supported by the National Key Research and Development Program of China [2017YFA0403804] and by the Fund of State Key Laboratory of

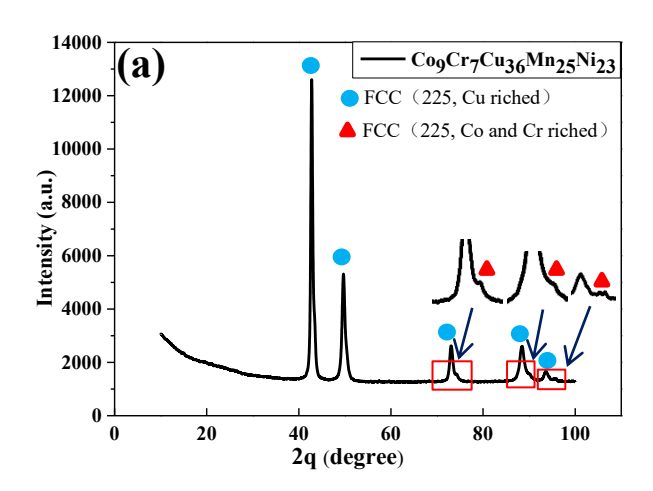
Advanced Welding and Joining.

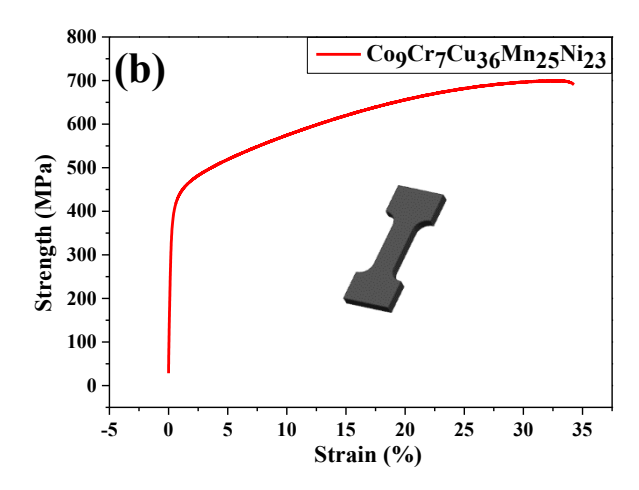
References

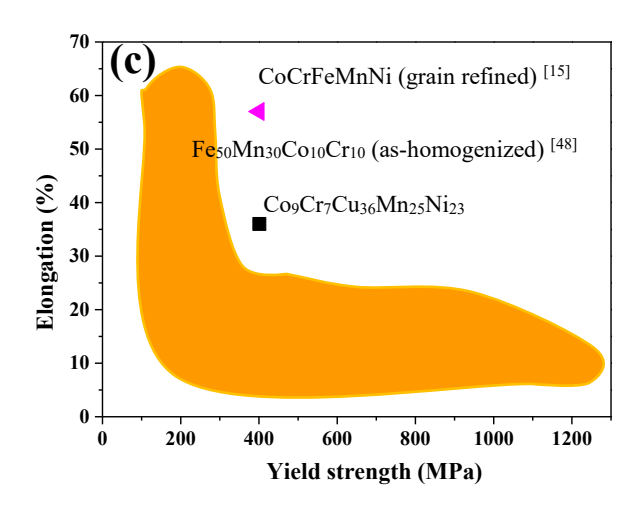
- [1]. Yeh, J-W, Chen S-K, Lin S-J, Gan J-Y, Chin T-S, Shun T-T, Tsau C-H, Chang S-Y. Nanostructured High-Entropy Alloys with Multiple Principal Elements: Novel Alloy Design Concepts and Outcomes. Advanced Engineering Materials. 6 (2004), 299-303.
- [2]. B Cantor, ITH Chang, P Knight, AJB Vincent. Microstructural development in equiatomic multicomponent alloys. Materials Science & Engineering A. 375-377 (2004), 213-218.
- [3]. Lim, XiaoZhi. Mixed-up metals make for stronger, tougher, stretchier alloys. Nature. 533 (2016), 306-307.
- [4]. Sun S J, Tian Y Z, Lin H R, X.G.Dong, Y.H.Wang, Z.J.Zhang, Z.F.Zhang. Enhanced strength and ductility of bulk CoCrFeMnNi high entropy alloy having fully recrystallized ultrafine-grained structure. Materials & Design. 133 (2017) 122-127.
- [5]. Yong Zhang, Ting Ting Zuo, Zhi Tang, Michael C. Gao, Karin A. Dahmene, Peter K. Liaw, Zhao Ping Lua. Microstructures and properties of high-entropy alloys. Progress in Materials Science. 61 (2014), 1-93.
- [6]. Yuan Liu, Yan Zhang, Heng Zhang, Naijuan Wang, Xiang Chen, Huawei Zhang, Yanxiang Li. Microstructure and mechanical properties of refractory HfMo0.5NbTiV0.5Six high-entropy composites. Journal of Alloys and Compounds. 694 (2017) 869-876.
- [7]. Zhang, Yan; Liu, Yuan; Li, Yanxiang; Microstructure and mechanical properties of a refractory HfNbTiVSi0.5 high-entropy alloy composite. Materials letter. 174 (2016) 174:82-85.
- [8]. Liu Yuan, Chen Min, Li Yanxiang, Chen Xiang. Microstructure and Mechanical Performance of AlxCoCrCuFeNi High-Entropy Alloys. Rare Metal Materials and Engineering. 38 (2009) 1602-1607.
- [9]. Y. Lu, Y. Dong, S. Guo, L. Jiang. H.J. Kang, T.M. Wang, B. Wen, Z.J. Wang, J. C. Jie. Z.Q. Cao. H.H Ruan. T.J Li, A promising new class of high-temperature alloys: Eutectic high-entropy alloys. Scientific Reports. 4 (2014) 6200.
- [10]. Lu Y, Gao X, Jiang L, et al. Directly cast bulk eutectic and near-eutectic high entropy alloys with balanced strength and ductility in a wide temperature range. Acta Materialia. 124 (2017) 143-150.
- [11]. Miracle D B, Senkov O N. A critical review of high entropy alloys and related concepts. Acta Materialia. 122(2016), 448-511.
- [12]. J.Y. He, W.H. Liu, H. Wang, Y. Wu, X.J. Liu, T.G. Nieh, Z.P. Lu. Effects of Al addition on structural evolution and tensile properties of the FeCoNiCrMn high-entropy alloy system. Acta Materialia. 62 (2014), 105-113.
- [13]. Mitsuharu Todai, Takeshi Nagase, Takao Hori, Aira Matsugaki, Aiko Sekita, Takayoshi Nakano. Novel TiNbTaZrMo high-entropy alloys for metallic biomaterials. Scripta Materialia, 129 (2017), 65-68.
- [14]. Sungwoo Sohn, Yanhui Liu, Jingbei Liu, Pan Gong, Silke Prades-Rodel, Andreas Blatter, B. Ellen Scanley, Christine C. Broadbridge, Jan Schroers. Noble metal high entropy alloys. Scripta Materialia, 126 (2017), 29-32.
- [15]. Gludovatz B, Hohenwarter A, Catoor D, Chang EH, George EP, Ritchie RO. A fracture-resistant high-entropy alloy for cryogenic applications. Science. 345(2014), 1153-158.
- [16]. J Joseph, N Stanford, P Hodgson, DM Fabijanic. Tension/compression asymmetry in additive manufactured face centered cubic high entropy alloy. Scripta Materialia. 129(2016), 30-34.
- [17]. D. Choudhuri, B. Gwalani, S. Gorsse, C.V. Mikler, R.V. Ramanujan, M.A. Gibson, R.Banerjee. Change in the primary solidification phase from fcc to bcc-based B2 in high entropy or complex concentrated alloys. Scripta Materialia. 127(2017), 186-190
- [18]. AE Karantzalis, A Poulia, E Georgatis, D Petroglou. Phase formation criteria assessment on the microstructure of a new refractory high entropy alloy. Scripta Materialia. 131 (2017), 51-54.
- [19]. ON Senkov, JD Miller, DB Miracle, C Woodward. Accelerated exploration of multi-principal element alloys with solid solution phases. Nature Communications. 6(2015), 6529.
- [20]. MH Tsai, JH Li, AC Fan, PH Tsai. Incorrect predictions of simple solid solution high entropy alloys: Cause and possible solution. Scripta Materialia, 127 (2017), 6-9.
- [21]. Zhang Y, Zhou Y, Lin J, G Chen, P Liaw, Solid-Solution Phase Formation Rules for Multi-component Alloys, Adv. Eng. Mater,

- 10 (2008) 534-538.
- [22]. Egami T, Waseda Y, Atomic size effect on the formability of metallic glasses, J Non-Cryst solids, 64 (1984) 113-134.
- [23]. Yang X, Zhang Y, Prediction of high-entropy stabilized solid-solution in multi-component alloys, Mater Chem Phys, 132 (2012) 233-238.
- [24]. Guo S, Liu C T, Phase stability in high entropy alloys: Formation of solid-solution phase or amorphous phase, Prog Nat Sci-Mater. 21 (2011) 433-446.
- [25]. Guo S, Ng C, Lu J, Liu C T, Effect of valence electron concentration on stability of fcc or bcc phase in high entropy alloys. J. Appl. Phys, 109 (2011) 645-647.
- [26]. Guo, S., Hu, Q., Ng, C., Liu, C.T. More than entropy in high-entropy alloys: forming solid solutions or amorphous phase. Intermetallics 41(2013) 96-103.
- [27]. Senkov O N, Miracle D B. A new thermodynamic parameter to predict formation of solid solution or intermetallic phases in high entropy alloys. Journal of Alloys & Compounds, 658(2016) 603-607.
- [28]. Tsai M H, Tsai K Y, Tsai C W, Lee C, Juan C C, Ye J W. Criterion for Sigma Phase Formation in Cr- and V-Containing High-Entropy Alloys. Materials Research Letters, 1(2013) 207-212.
- [29]. Tsai M H, Chang K C, Li J H, Tsai R C, Cheng A H. A second criterion for sigma phase formation in high-entropy alloys. Materials Research Letters, 4(2016) 1-6.
- [30]. Troparevsky M C, Morris J R, Kent P R C, Lupini A R, Stocks G M. Criteria for Predicting the Formation of Single-Phase High-Entropy Alloys. Physical Review X, 5(2015), 1-6.
- [31]. Yurchenko N, Stepanov N, Salishchev G. Laves-phase formation criterion for high-entropy alloys. Metal Science Journal, 33(2016)
- [32]. N Zhou, T Hu, J Huang, J Luo. Stabilization of nanocrystalline alloys at high temperatures via utilizing high-entropy grain boundary complexions. Scripta Materialia, 124 (2016), 160-163.
- [33]. Z. G Zhu, KH Ma, X Yang, CH Shek. Annealing effect on the phase stability and mechanical properties of (FeNiCrMn)_(100-x)Co_x high entropy alloys. Journal of Alloys & Compounds, 695(2017), 2945-2950.
- [34]. J. Q. Yao, X.W. Liu, N. Gao, Q.H. Jiang, N. Li, G. Liu, W.B. Zhang, Z.T. Fan, Phase stability of a ductile single-phase BCC Hf0.5Nb0.5Ta0.5Ti1.5Zr refractory high-entropy alloy, Intermetallics. 98 (2018) 79–88.
- [35]. Ma LL, Li C, Jiang YL, Zhou JL, Wang L, Wang FC, Cao TQ, Xue YF. Cooling rate-dependent microstructure and mechanical properties of Al_xSi_{0.2}CrFeCoNiCu_{1-x} high entropy alloys. Journal of Alloys & Compounds, 694(2017), 61-67.
- [36]. Tsai M H, Fan A C, Wang H A. Effect of atomic size difference on the type of major intermetallic phase in arc-melted CoCrFeNi_X high-entropy alloys. Journal of Alloys & Compounds, 695(2017), 1479 1487.
- [37]. Wenyi Huo, Hui Zhou, Feng Fang, Xianjun Hu, Zonghan Xie, Jianqing Jiang. Strain-rate effect upon the tensile behavior of CoCrFeNi high-entropy alloys. Materials Science & Engineering A, 689 (2017), 366–369.
- [38]. N. Liu, P.H. Wu, P.J. Zhou, Z. Peng, X.J. Wang, Y.P. Lu. Rapid solidification and liquid-phase separation of undercooled CoCrCuFexNi high-entropy alloys. Intermetallics, 72(2016), 44-52.
- [39]. Takeuchi A, Inoue A. Classification of bulk metallic glasses by atomic size difference, heat of mixing and period of constituent elements and its application to characterization of the main alloying element. Mater. Trans. 46 (2006) 2817–2829.
- [40]. K. Guruvidyathri, K.C. Hari Kumar, J.W. Yeh, B.S. Murty. topologically Close-packed Phase Formation in High Entropy Alloys: A Review of Calphad and Experimental Results. JOM. 69 (2017) 2113–2124.
- [41]. Rui Feng, Michael C. Gao, Chanho Lee, Michael Mathes, Tingting Zuo, Shuying Chen, Jeffrey A. Hawk, Yong Zhang, Peter K. Liaw. Design of Light-Weight High-Entropy Alloys. Entropy. 18(2016) 333.
- [42]. Y. Zhang, Z.P. Lu, S.G. Ma, P.K. Liaw, Z. Tang, Y.Q. Cheng, M.C. Gao. Guidelines in predicting phase formation of high-entropy alloys. Mrs Commun. 42 (2014) 57–62.
- [43]. R Chen, G Qin, H Zheng, LWang, Y Su, Y L Chiu, H Ding, J Guo, H Fu. Composition design of high entropy alloys using the valence electron concentration to balance strength and ductility. Acta Mater. 144 (2018) 129–137.

- [44]. G Qin, S Wang, R Chen, X Gong, L Wang, Y Su, J Guo, H Fu. Microstructures and mechanical properties of Nb-alloyed CoCrCuFeNi high-entropy alloys. J Mater Sci Technol. 34 (2018) 365–369.
- [45]. G Qin, W Xue, C Fan, R Chen, L Wang, Y Su, H Ding, J Guo. Effect of Co content on phase formation and mechanical properties of (AlCoCrFeNi)100-xCox high-entropy alloys. Mater. Sci. Eng. A. 710 (2018) 200–205.
- [46]. Rao Z Y, Wang X, Zhu J, Chen X H, Wang L, Si J J, Wu Y D, Hui X D. Affordable FeCrNiMnCu high entropy alloys with excellent comprehensive tensile properties. Intermetallics. 77 (2016) 23–33.
- [47]. Zhang L, Zhou Y, Jin X, Du X, Li B. The microstructure and high-temperature properties of novel nano precipitation-hardened face centered cubic high-entropy superalloys, Scr. Mater. 146 (2018) 226–230.
- [48]. Zhiming L, Konda G P, Yun D, Dierk R, Tasan C C. Metastable high-entropy dual-phase alloys overcome the strength–ductility trade-off. Nature. 534 (2016) 227–230.
- [49]. Deng Y, Tasan C C, Pradeep K G, Springer H, Kostka A, Raabe D. Design of a twinning-induced plasticity high entropy alloy. Acta Mater. 94 (2015) 124–133.
- [50]. W H Liu, Z P Lu, J Y He, J H Luan, Z J Wang, B Liu, Y Liu, M W Chen. Ductile CoCrFeNiMox high entropy alloys strengthened by hard intermetallic phases. Acta Mater. 116 (2016) 332–342.
- [51]. Liu W H, J Y He, H L Huang, H Wang, Z P Lu, C T Liu. Effects of Nb additions on the microstructure and mechanical property of CoCrFeNi high-entropy alloys. Intermetallics 60(2015) 1–8.
- [52]. Xi Jin, Yang Zhou, Lu Zhang, Xingyu Du, Bangsheng Li. novel Fe20Co20Ni41Al19 eutectic high entropy alloy with excellent tensile properties. Materials Letters. 216 (2018) 144–146.
- [53]. Tilak Bhattacharjee, Ruixiao Zheng, Yan Chong, Saad Sheikh, Sheng Guo, Ian Thomas Clark, Toshiro Okawa, Irfan Samad Wani, Pinaki Prasad Bhattacharjee, Akinobu Shibata, Nobuhiro Tsuji. Effect of low temperature on tensile properties of AlCoCrFeNi2.1eutectic high entropy alloy. Materials Chemistry and Physics. 210 (2018) 207–212.







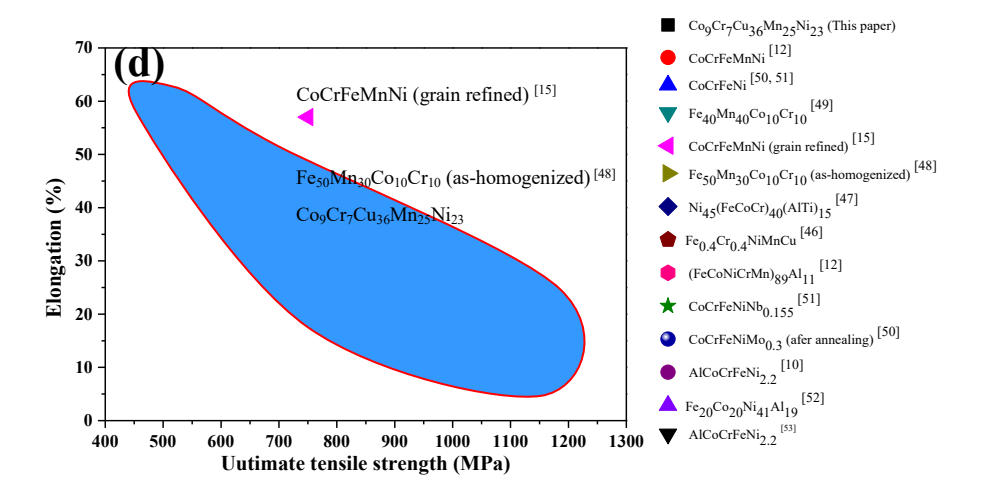


Figure. 1. Mechanical behavior and crystal structure of Co₉Cr₇Cu₃₆Mn₂₅Ni₂₃ HEA. (a) XRD patterns. (b) Tensile engineering stress-strain curve. (c) The tensile yield strength and elongation for the Co₉Cr₇Cu₃₆Mn₂₅Ni₂₃ HEA and other HEAs [12, 15, 16, 19, 26, 45-49, 64, 65]. (d) The ultimate tensile strength and elongation for the Co₉Cr₇Cu₃₆Mn₂₅Ni₂₃ HEA and other HEAs [12, 15, 16, 19, 26, 45-49, 64, 65].

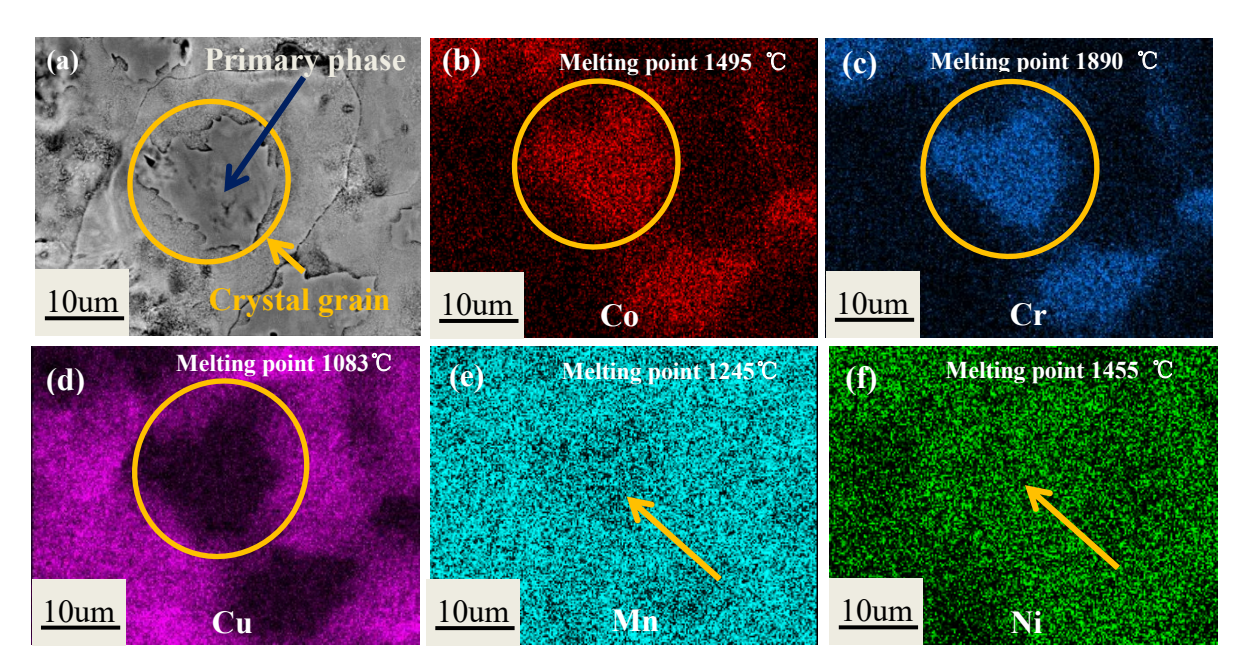


Figure. 2. Microstructure and elements distribution maps of Co₉Cr₇Cu₃₆Mn₂₅Ni₂₃ HEA through EDS. (a)

Microstructure of Co₉Cr₇Cu₃₆Mn₂₅Ni₂₃ HEA. (b-f) Elements distribution maps of Co, Cr, Cu, Mn and Ni in

 $Co_{9}Cr_{7}Cu_{36}Mn_{25}Ni_{23}\ HEA.$

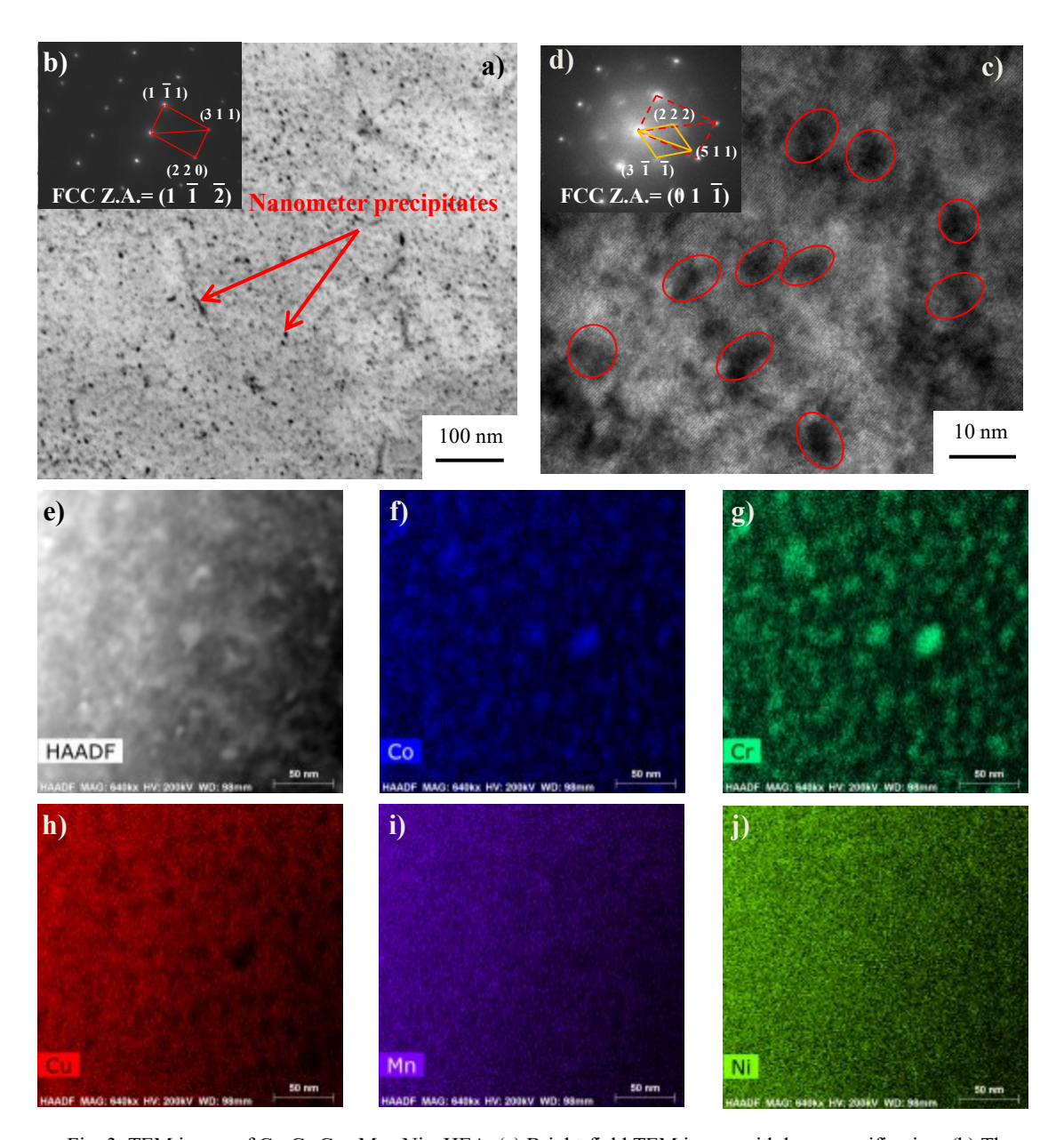


Fig. 3. TEM image of Co₉Cr₇Cu₃₆Mn₂₅Ni₂₃ HEA. (a) Bright-field TEM image with low magnification. (b) The electron diffraction spot of a. (c) Bright-field TEM image with high magnification. (d) The electron diffraction spot of c. (e-j) High-angle annular dark-field (HAADF) image and the corresponding STEM-EDS elemental maps of Co, Cr, Cu, Mn, and Ni.

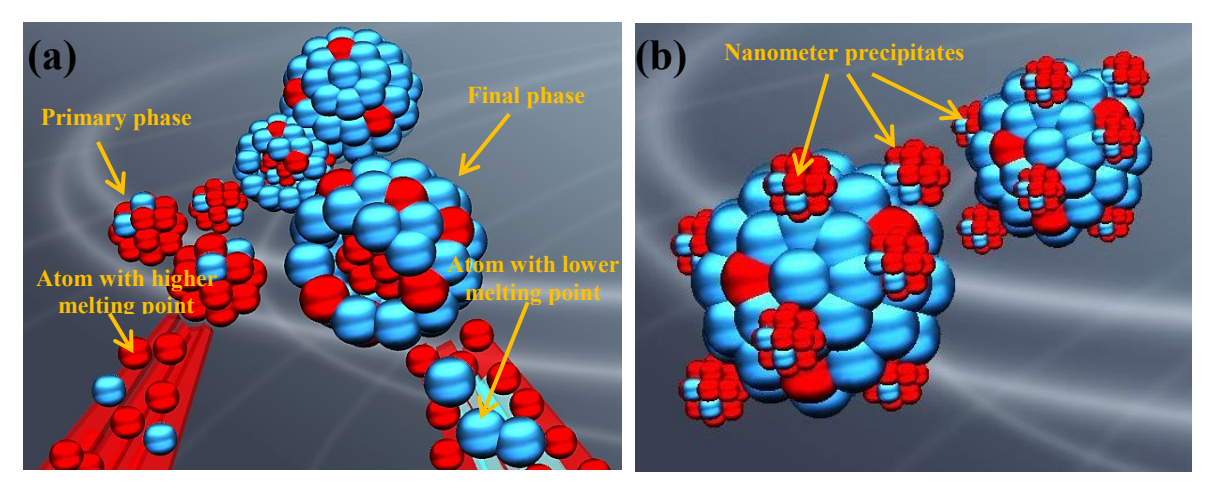


Fig. 4 (a). Atom motion model of the crystal-forming behavior of Co₉Cr₇Cu₃₆Mn₂₅Ni₂₃ HEA. Co, Cr, and Ni atoms have higher melting points as compared to Cu and Mn atoms, which have lower melting points in the proposed HEA system. (b). The forming behavior of nanometer precipitates.